Chapter 3

Biosensing Activity of C_{24} Fullerene towards DNA Nucleobases

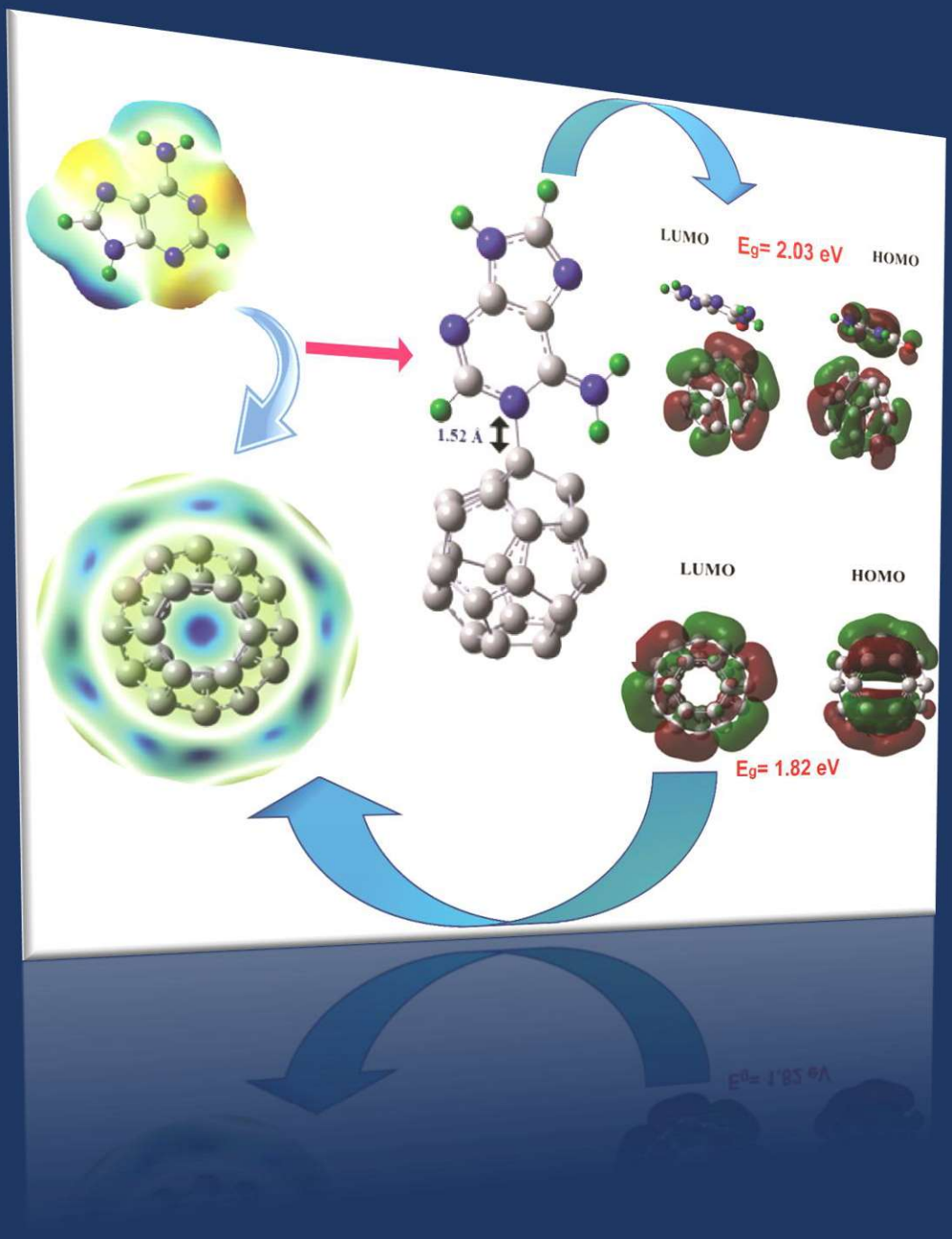

3.1 Introduction

Sensors have constantly garnered acclaim for their wide range of applications in fields such as innovation, equipment manufacturing, medicinal research, and environmental surveillance. A particular role of biosensors is to recognize biological molecules like proteins, peptides, DNA, and RNA and convert their biorecognition events into electrical and optical signals to determine the quantity of the target [1-2]. Forensic sciences, genomics systems, food safety, environmental monitoring, and medicinal research all use nucleotide sensing and sequencing as an emerging sector for illness detection [3]. It has several uses, including the identification of toxins, microbial infections in food analysis, and cancer-associated genes. It has several uses, including the identification of toxins, microbial infections in food analysis, and cancer-associated genes [4]. The integration of electrochemical biosensors with nanomaterials, which improves their performance and sensitivity, is essential to their development. Nanomaterials essentially serve as recognition agents for enzymes, antibodies, DNA, RNA, and other proteins in biosensors by their contact with or affinity towards these biomolecules. Affinity-based biosensors are those that solely interact with the sensor surface, as opposed to catalytic sensors, which alter or destroy biomolecules on the sensor surface. As a result, prior to biosensor device manufacturing, the interaction between nanomaterials and biomolecules is crucial [5-6].

Due to its earthly abundance, low cost, and presence of allotropes with distinct characteristics, the family of carbon nanostructures is one of the substitutes for the fundamental electrical sensors [7]. Because of their unique structural, electronic, chemical, optical, and sensing characteristics, graphene and graphene oxide, which are renowned as prominent members of the sp^2 hybridized carbon allotrope family, along with one-dimensional materials [8] and zero-dimensional structures [9], have found widespread applications across a multitude of fields [10-12]. These applications span a wide range of fields, including biology, medicine, and pharmaceuticals. The initial discovery of a carbon nanomaterial was C_{60} fullerene, synthesized experimentally by H. Kroto in 1985 [13]. Owing to its hydrophobic nature, biocompatibility, substantial surface area resulting from its spherical structure, and its relatively lower toxicity towards living microorganisms [14], fullerene has garnered significant attention in the biomedical sector when compared to graphene and carbon nanotubes (CNTs). It has also been successfully used as a biosensor for DNA nucleobase. Experimental evidence suggests that it is capable of concurrently sensing adenine and guanine [15]. Following that, it was

discovered that fullerene made a strong option for DNA-based sensors due to its unique hydrophobic nature. Because of its special hydrophobic properties, it is more readily soluble in organic solvents than it is in polar ones. It benefits from maintaining the better electrochemical behaviour towards biomolecules combined with strong electron affinity and ionisation potential for interaction [16]. Fullerene isomers including C_{20}, C_{24}, and C_{60} have recently emerged as some of the most effective suitable materials for biological applications like biosensing [17-18], drug delivery [19-20] and antibacterial activity [21]. Strain-induced pentagon-pentagon fusions render the smallest C_{20} fullerene unstable. As a potential DNA biosensor, the C_{24} fullerene has not been studied despite being more stable. The introduction of dopant elements such as Cr and/or Ni led to enhanced stabilization of C_{20} fullerene, resulting in improved adsorption capabilities for adenine, guanine, cytosine, thymine, and uracil [22]. Among the various C_{24} configurations, the fullerene exhibiting D6d symmetry is established as the most robust, demonstrating effective utility as a carrier for drug adsorption. It has proven particularly successful in adsorbing anticancer drugs like melphalan, 5-fluorouracil, and chlormethine, as well as drugs containing ephedrine [23-24]. Furthermore, in order to explore the interaction between $[M(H_2O)_6]^{2+}$ ($M = Ca^{2+}, Zn^{2+}$) cations and ensure the long-term stability of both C_{24} and C_{36} nanocages, a comprehensive investigation was conducted. This investigation encompassed both DFT studies and MD simulations of C_{24} and C_{36} fullerenes [25].

In the current study, we want to better understand how the C_{24} nanocage reacts with nucleobases such as adenine (A), thymine (T), guanine (G), cytosine (C), and uracil (U). In order to do this, we have investigated the structural and electrical characteristics both before and after the adsorption of the five nucleobases over the C_{24} nanocage. In order to anticipate the character of interactions between nucleobases and C24, and to assess its potential as a DNA sensor, we examined aspects such as NBO charge transfer analysis, alterations in the energy gap, dipole moment changes, and recovery times.

3.2 Computational details

All of the nucleobases, C_{24} fullerene, and quantum theoretical calculations are geometrically optimised using the DFT/B3LYP using the D3 version of Grimme's dispersion (GD3) [26] utilising the 6-31G(d,p) basis set, respectively, with the Gaussian 09 package[27]. Since the C_{24} has already been proved to be the most stable at neutral charge and multiplicity

one, we have optimised it [28]. Following that, the nucleobase are neutral molecules devoid of charges; via the optimisation calculations, we have chosen global charge zero, which is as neutral with multiplicity one. The adsorption energy, E_{ad}, is described as

$$E_{ad} = E_{C24/nucleobase} - (E_{C24} + E_{nuleobase}) \text{ -----(1)}$$

Whereas $E_{nucleobase}$ and $E_{C24/nucleobase}$ are the energies of the isolated nucleobases and the relaxed C_{24} nanocage with the adsorbed nucleobases molecule, respectively, and E_{C24} corresponds to the energy of the relaxed C_{24} fullerene. The HOMO-LUMO energy gap (E_G), measured between the highest molecular orbital (HOMO) and lowest unoccupied molecular orbital (LUMO), is computed from,

$$E_G = E_{LUMO} - E_{HOMO} \text{ ------(2)}$$

3.3 Results and Discussion

3.3.1 Optimized geometry of the adsorbent C_{24} fullerene and nucleobases

Understanding the behavior of biosensors requires thorough research of the structural and electrical characteristics of C_{24} fullerene and nucleobases. We initially optimized C_{24} fullerene and all relevant nucleobases (adenine (A), thymine (T), guanine (G), cytosine (C), and uracil (U)), which are depicted in Fig. 1. The C_{24} fullerene displays the D_{6h} point group, and the structure contains 12 pentagonal rings in the middle, one hexagonal ring at the top, and one at the bottom (see **Figure 3.1**). The reported C_{24} fullerene bond lengths are 1.52 (C-C) and 1.36 (C=C), and the energy gap (E_G) is 1.84 eV with the HOMO and LUMO energies being -5.65 eV and -3.83 eV, respectively (see **Table 3.1**). There is a fair amount of concordance between the calculated bond lengths and E_G and earlier studies [23]. The cohesive energy calculation results in a cohesive energy value of -8.22 eV/atom, which is used to estimate the structural stability of C_{24}. Its stability is shown by the high and negative cohesive energy value, which is in line with earlier research [29]. To assure stability with IR spectra frequencies, the vibrational modes have also been researched. The frequency ranges of 200 to 1600 cm^{-1} for all vibrational modes are real, and this is also compatible with the research of Hossian et al. [29]. We optimized the nucleobases after confirming the C_{24} fullerene's ground state characteristics. We require a precise characterization of the charge distribution of the molecules in order to understand the affinities and interactions of nucleobases with fullerene C_{24}. As a result, the computed Electrostatic Potential (ESP) of the nucleobases under consideration and C_{24}

fullerene is shown in **Figure 3.2** [30]. The color scheme has been designed such that areas with attractive potential seem red and areas with repellent potential appear blue. The hollow portions of the pentagonal and hexagonal sides of the C_{24} fullerene are covered by intermediate

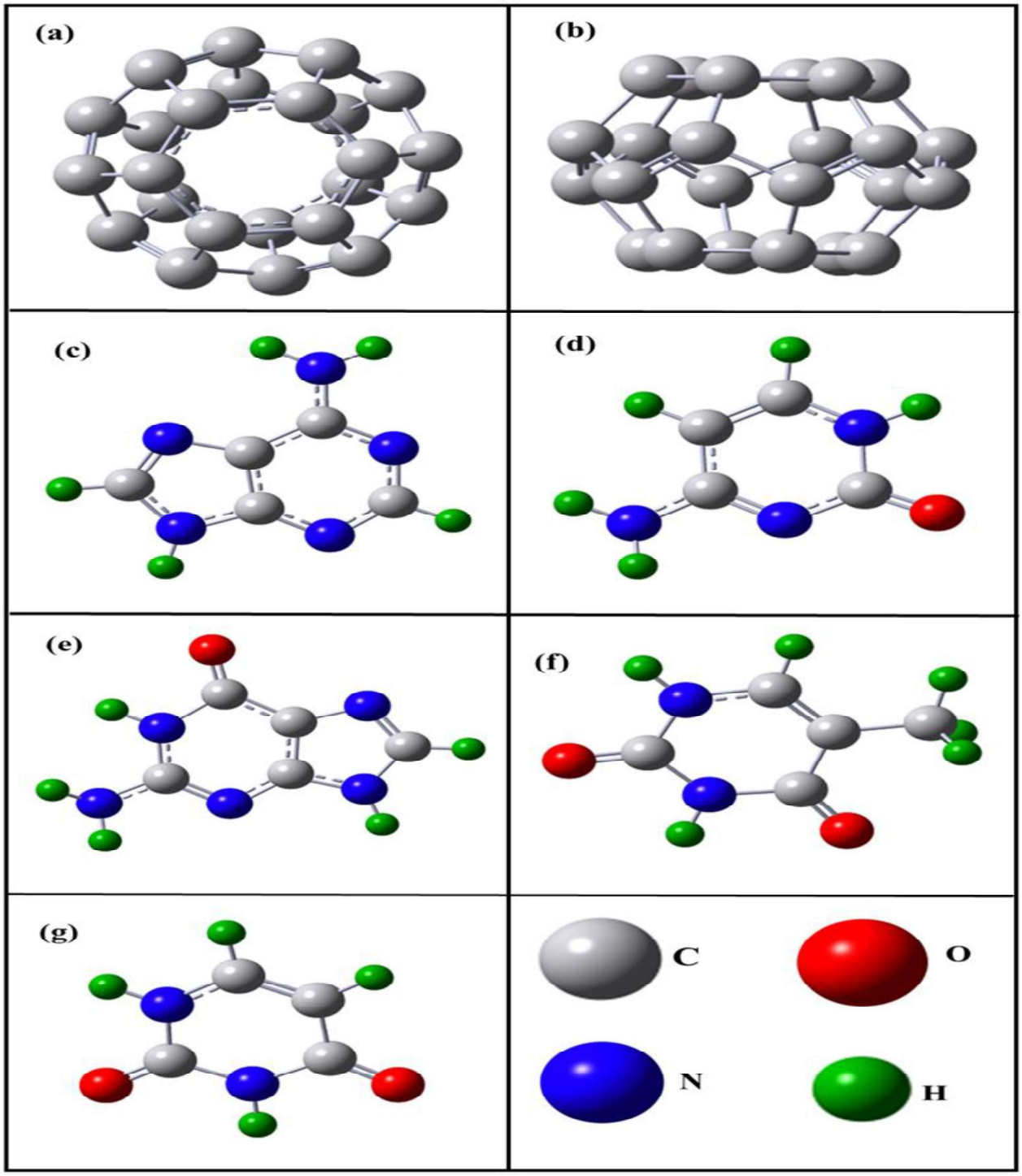

Figure 3.1: *The optimized geometrical arrangement of C_{24} fullerene (depicted in both top (a) and side view (b)), along with the nucleobases Adenine (c), Cytosine (d), Guanine (e), Thymine (f), and Uracil (g).*

negative regions. It is appropriate for nucleophilic attack sites since we found positive potential at the top of C_{24}'s hexagonal and pentagonal sides. We have found that the nitrogen atom attached to the all-nucleobase molecules has negative potential areas (red zone) close by, making it an electrophilic attack site. To address this issue, we strategically directed the electrophilic attack site of the nucleobases toward the nucleophilic attack site of C_{24} fullerene. When the implicit water model is used as the solvent, no discernible change in the ESP of C_{24} fullerene or any of the nucleobases is seen [30].

3.3.2 Interaction properties of Adenine(A), Cytosine(C), Guanine(G), Thymine(T), and Uracil (U) adsorbed onto C_{24} fullerene

We thoroughly investigated the adsorption of the most stable arrangements of Adenine, Cytosine, Guanine, Thymine, and Uracil molecules on C_{24} fullerene, as illustrated in Figure 3.3. This analysis aimed to affirm the potential of C_{24} fullerene as an effective affinity-based DNA sensor. The C_{24} fullerene interacts solely with nucleobases; nucleobases do not deform or deteriorate, as has been established. The C_{24} fullerene's hexagonal or pentagonal sites can both receive the nucleobase adsorptive attachments. Different adsorption locations for the nucleobase molecules over the C_{24} fullerene were first suggested in an effort to determine the lowest energy arrangement. Due to the extra electrons present in comparison to H-atoms, adenine prefers to be adsorbed over the top of the C_{24} fullerene through N-atom, which is compatible with ESP analysis. The Adenine molecule adsorbs to the C_{24} nanocage with an energy of -1.16 eV, and the distance between the nitrogen (N) atom of Adenine and the carbon atom of C_{24} is approximately 1.52 Å (see Table 1). Strong chemisorption occurs as a result of the adenine molecule's adsorptive attachment to the C_{24} fullerene [31]. The pentagonal location of the C_{24} fullerene experienced cytosine adsorption with an absorption value of -0.42 eV. Its physisorption nature is shown by the minimal atom-to-atom distance of 2.38 Å between the Cytosine and C_{24} fullerene [32]. The adsorption energies of the guanine and thymine molecules, which are -0.38 eV and -0.32 eV, respectively, are applied during the physisorption process over the pentagonal site of the C_{24} fullerene. Guanine and C_{24} fullerene have an atom-to-atom minimum distance of 2.79 Å, whereas Thymine and C_{24} fullerene have a 3.28 Å minimum. With an adsorption energy of -0.3 eV, the Uracil underwent a mild physisorption process of adsorption over the hexagonal site of the C_{24} fullerene. Uracil and C_{24} fullerene are separated from one another by a minimum of 3.30 Å, and there is van der wall contact between them. Five nucleobases were used to explore the adsorption energy and interaction distances across

Table 3.1: *Calculated value of Adsorption energy (E_{ad}), LUMO energy (E_{LUMO}), Fermi level (E_F), HOMO energy (E_{HOMO}), HOMO-LUMO gap (E_G), relative change in E_F (ΔE_{FR}), relative change in E_G (ΔE_{GR}) and adsorption distance(d) of Adenine, Cytosine, Guanine, Thymine, and Uracil adsorbed over C_{24} fullerene, respectively.*

System	E_{ad} (eV)	E_{LUMO} (eV)	E_F (eV)	E_{HOMO} (eV)	E_G (eV)	ΔE_{FR} (%)	ΔE_{GR} (%)	d (Å)
C_{24}	….	-3.83	-4.74	-5.65	1.82	……	…..	…….
A/C_{24}	-1.16	-2.51	-3.53	-4.54	2.03	25.31	11.6	1.52
C/C_{24}	-0.42	-3.05	-4.00	-4.95	1.9	15.61	4.4	2.38
G/C_{24}	-0.377	-3.88	-4.739	-5.59	1.71	0.21	-5.6	2.79
T/C_{24}	-0.324	-3.84	-4.77	-5.69	1.85	-0.63	1.64	3.28
U/C_{24}	-0.301	-3.91	-4.82	-5.72	1.81	-1.68	-0.54	3.30

the C_{24} fullerene, and it is clear from the results that the stronger the relationship between them is, the shorter the adsorption distance correlates to the stronger adsorption energy. Adsorption happens in the following order. The adsorption sequence can be summarized as A > C > G > T > U, as illustrated in **Table 3.1**. Notably, there is not a substantial disparity in the adsorption energy among G, T, and U. The type of adsorption and the sequence or propensity of the nucleobase towards the fullerene are only qualitatively expressed by the adsorption energy. We have carried out the NBO analysis and the Mulliken charge analysis to comprehend the quantum mechanical reason for this propensity of nucleobases towards the fullerene.

3.3.3 The natural bond orbital (NBO) charge analysis

One of the key elements in establishing the superiority of an adsorbate over an adsorbent is electron charge transfer. Furthermore, we explored the charge transfer between the C_{24} fullerene and the five nucleobases in their equilibrium geometries throughout the adsorption process through the application of natural bond orbital computations [33]. Additionally, the charge transfer between the C_{24} fullerene and five nucleobases in the equilibrium geometries of the adsorption process has been investigated using natural bond

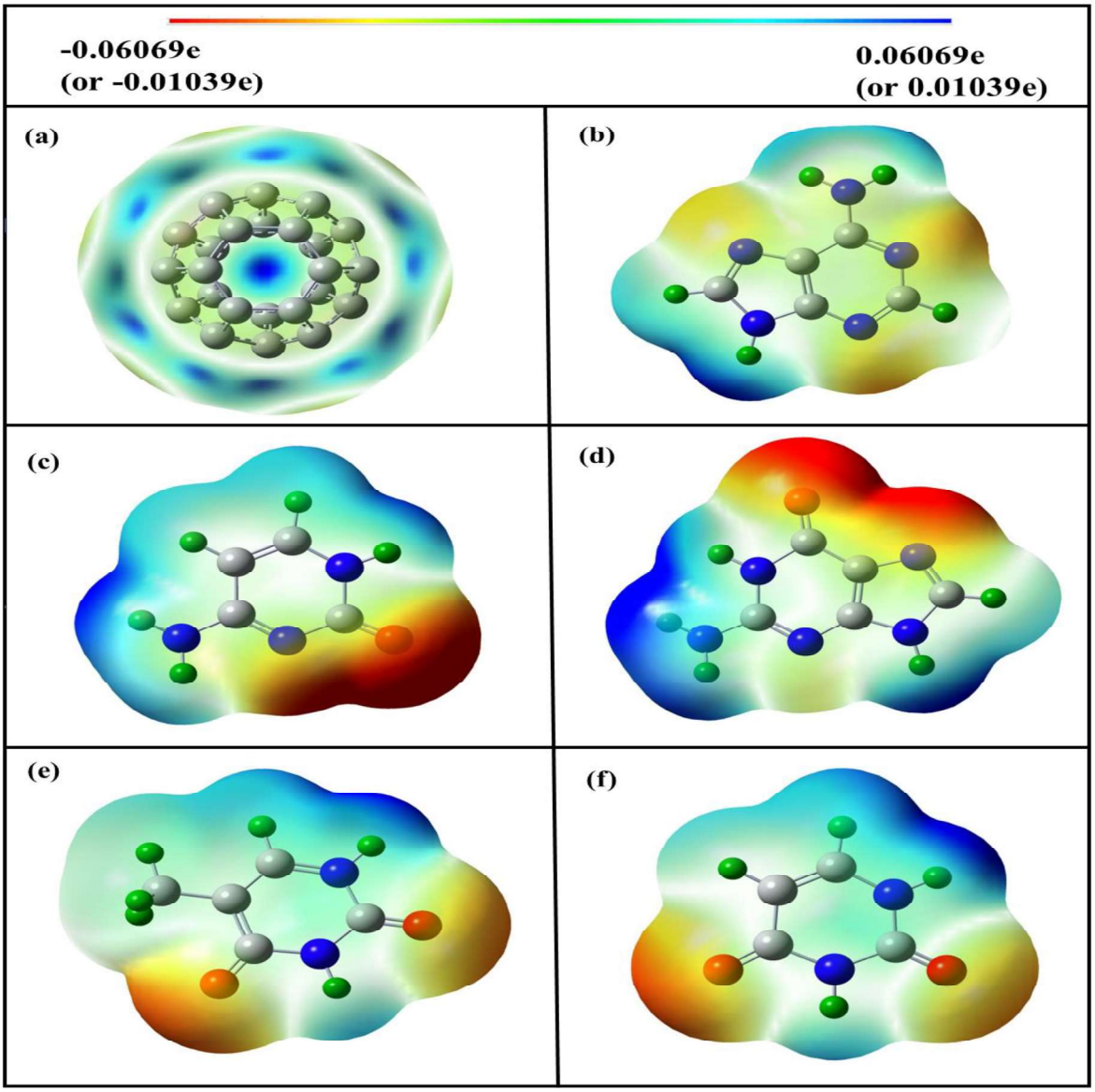

Figure 3.2: *Electrostatic potential (ESP) maps were generated for C_{24} fullerene (depicted in (a)) and for the nucleobases, including Adenine (b), Cytosine (c), Guanine (d), Thymine (e), and Uracil (f) (with EPS ranging from -0.06069e to 0.06069e).*

orbital calculations [33-35], and the outcomes of the NBO study are shown in **Table 3.2**. We have examined the Mulliken population to ascertain the direction of spontaneous electron flow for the examined intermolecular interactions [31][36-37]. The total Mulliken charge on the nucleobase molecules is discovered to be +0.395e, +0.112e, +0.016e, +0.025e, and -0.027e, respectively, when the nucleobase molecules of adenine, cytosine, guanine, thymine, and uracil

adsorb over C_{24} fullerene. Since the total Mulliken charge of isolated nucleobase molecules is zero, the negative Mulliken charge for uracil indicates that charge transfer occurs from

Table 3.2: *The NBO second-order perturbation energy (E^2, measured in kcal/mol) signifies the extent of charge transfer occurring between C_{24} fullerene and each of the nucleobases: Adenine, Cytosine, Guanine, Thymine, and Uracil.*

System	Donor	Acceptor	E^2 (Kcal/mol)
A/C_{24}	BD (C_3 - C_5)	BD* (N_{35} – H_{39})	32.17
C/C_{24}	BD (C_{11} – C_{14})	BD* (N_{31} – H_{32})	2.08
G/C_{24}	BD (C_{20} – C_{21})	BD* (N_{35} – H_{38})	0.60
T/C_{24}	BD (C_{16} – C_{17})	BD* (C_{26} – O_{34})	0.49
U/C_{24}	BD (C_{18} – C_{19})	BD* (C_{36} – H_{38})	0.29

nucleobase to C_{24} fullerene, whereas charge transfer from C_{24} fullerene to other nucleobases (A, C, and T) has been observed [36-37]. **Figure 3.4** displays the charge distribution of the nucleobase molecules adsorbed on C_{24} fullerene. The NBO technique has also been carefully examined to clarify the charge transfer between the C_{24} fullerene and nucleobases. Here, the second-order Fock matrix's donor-acceptor (bond-antibond) interaction's stabilization energy for second-order perturbations, $E^{(2)}$, has been evaluated using the NBO computation [30][38]. The delocalization of the donor (i) to the acceptor (j) results in the second order perturbation stabilization energy, $E^{(2)}$, being given as

$$E^{(2)} = \Delta E_y = q_i \frac{F^{(2)}(ij)}{\varepsilon_i - \varepsilon_j} \text{ ---------- (3)}$$

The second order perturbation stabilization energy is known to be inversely correlated with the NBO interacting strength, and a greater stabilization energy denotes a stronger donor–acceptor interaction and better stability for the C_{24}/nucleobase complexes. Only the maximum values of $E^{(2)}$ were included in **Table 3.1**. The acquired results show that the A/C_{24} complex's intermolecular interaction identifies π(C3-C5) of C_{24} fullerene as the donor and π^*(N_{35}-H_{39}) of adenine as the acceptor, which is compatible with ESP findings. In addition, the most

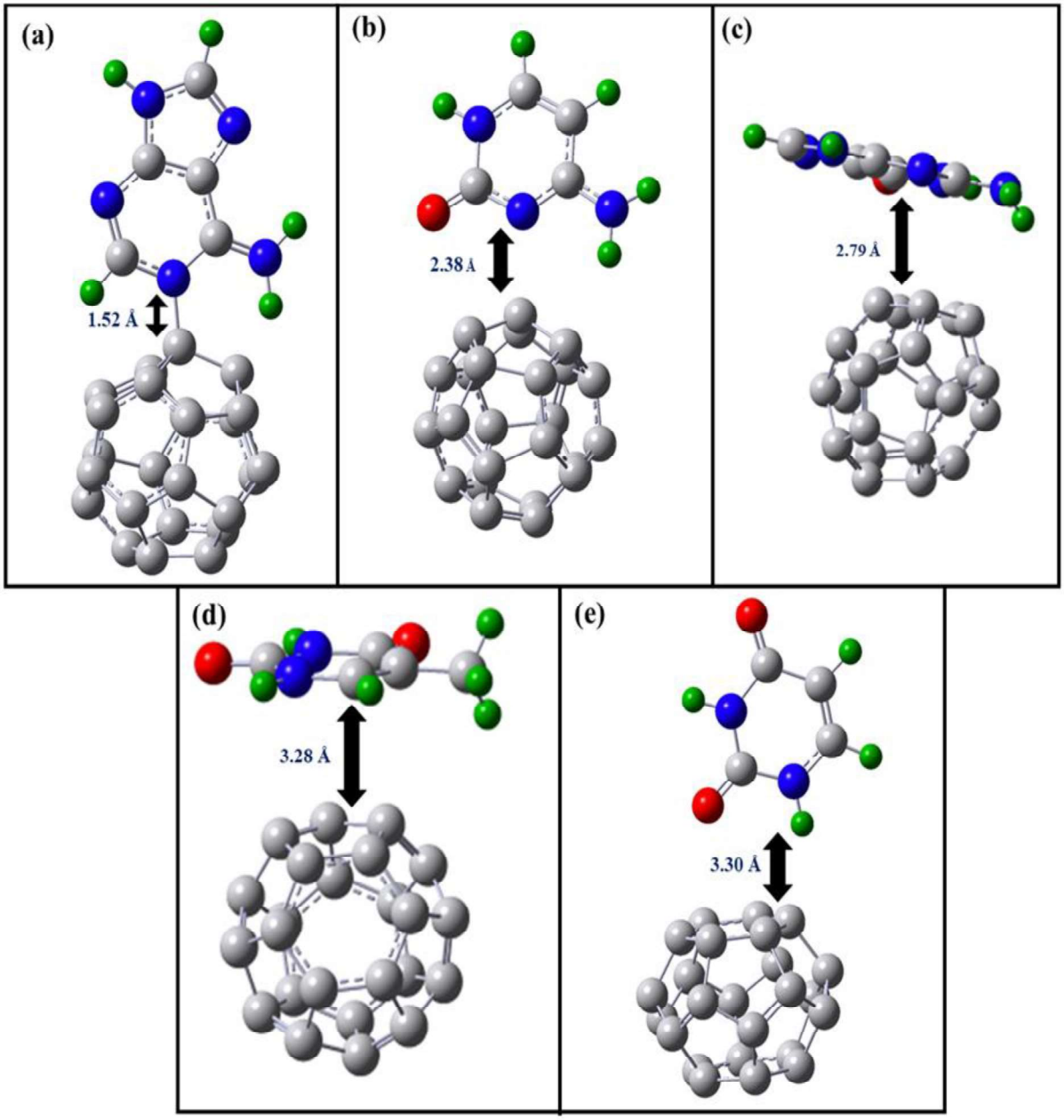

Figure 3.3 ***:*** *The most energetically favourable configurations of Adenine (a), Cytosine (b), Guanine (c), Thymine (d), and Uracil (e) adsorbed onto C_{24} fullerene, respectively.*

significant contact between the C_{24} fullerene and the adenine is shown by the highest value of $E^{(2)}$, which is 32.17 kcal/mol. It is clear that the adsorption mechanism is chemisorption in nature from the charge transfers and adenine's adsorption energy over C_{24}. The maximal $E^{(2)}$ values for C/C_{24}, G/C_{24}, T/C_{24}, and U/C_{24} complexes are 2.08, 0.6, 0.49, and 0.49 Kcal.mol^{-1},

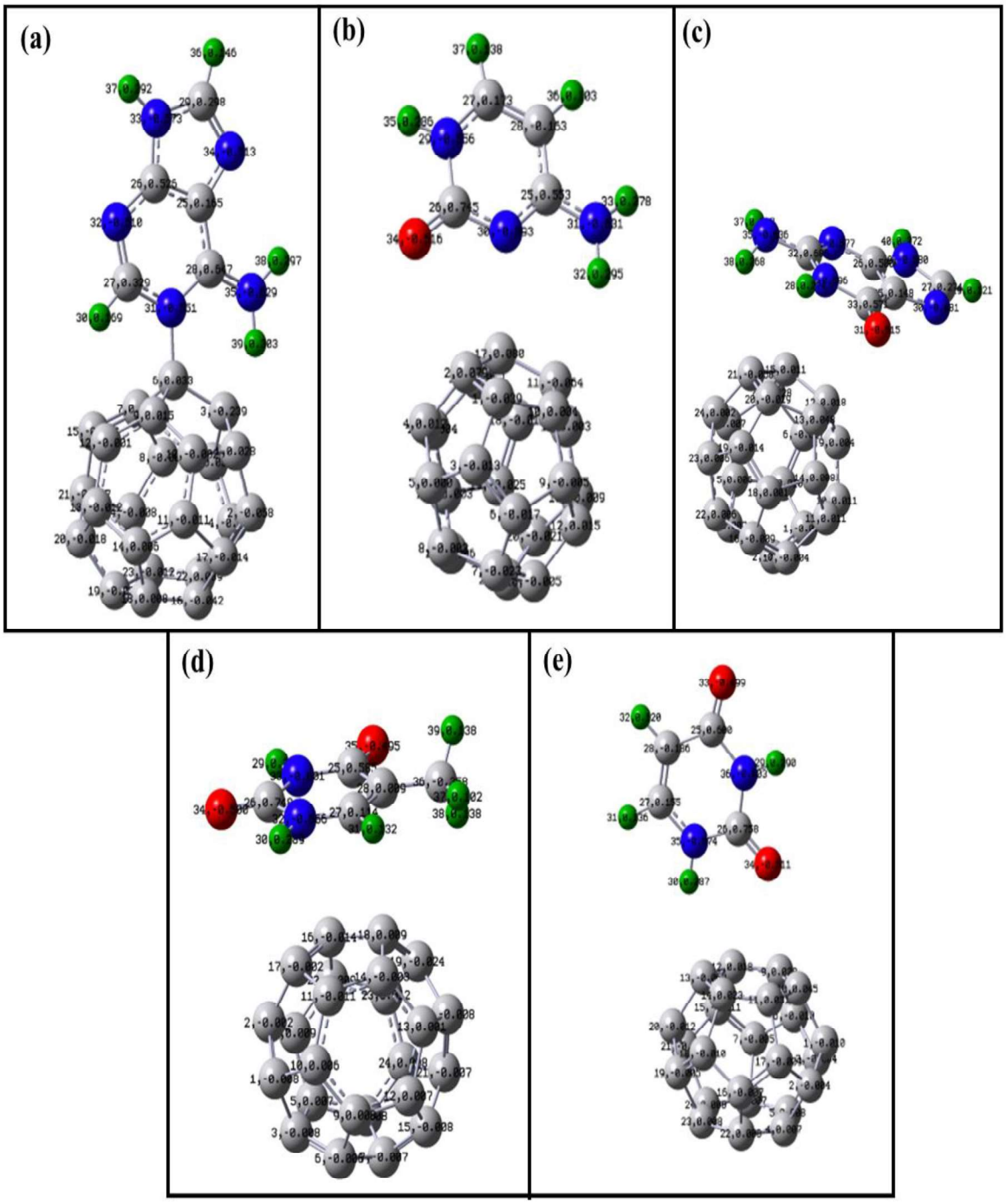

Figure 3.4: *Mulliken charge population assessment for Adenine (a), Cytosine (b), Guanine (c), Thymine (d), and Uracil (e) when adsorbed onto C_{24} fullerene, respectively.*

respectively. The lower values support the physisorption character of the adsorption between these molecules. In general, one may state that the interaction happens between the pure C_{24}

fullerene molecule's π orbitals, which function as the donor, and the nucleobase molecules' π^* orbitals, which serve as the acceptor.

3.3.4 Density of States (DOS)

In order to get a better understanding of the interaction between the nucleobase molecules and C_{24} fullerene, we computed the LUMO energy (E_{LUMO}), Fermi level (E_F), HOMO energy (E_{HOMO}), HOMO-LUMO gap (E_G), relative change in E_F (E_{FR}), and relative change in E_G (E_{GR}), which are all reported in **Table 3.1**. From the energy levels of the HOMO-LUMO molecular orbits, we may additionally derive an electronic transition and a global reactivity descriptor. The energy gap, according to Koopmans' theorem, is directly connected to chemical reactivity; the lower the energy gap, the greater reactivity (stability); in contrast, the energy of HOMO and LUMO is related to ionization potential ($-E_{HOMO}$) and electron affinity ($-E_{LUMO}$). C_{24} fullerene is more reactive than C_{60}, C_{20}, or even doped-C_{20} fullerenes because its energy gap is less [39-40]. It is a better candidate for use in DNA biosensors because its lower ionization potential (5.56 eV) than those of C_{60} [39], C_{20}, and doped C_{20} [40] fullerenes suggest a lower energy requirement to remove the majority of loosely bound electrons and a higher electron affinity (3.83 eV) in comparison to them. While E_G decreases by roughly 5.49% (1.72 eV) in the case of guanine adsorption, there is a considerable shift in Fermi energy and a significant rise in E_G for the adenine/cytosine adsorption over C_{24} fullerene, confirming their interaction. Moreover, this assertion can be substantiated by the heightened intensity of bonding states following the adsorption of Adenine and Cytosine onto C_{24} in contrast to its pristine form. Conversely, when Thymine and Uracil are adsorbed onto C_{24} fullerene, there is no abrupt shift in the Fermi energy, and the disparity in E_G is merely under 3% eV compared to the original C_{24}. This underscores the physisorption characteristic of the adsorption process, a conclusion supported by the slight alteration in bonding states evident in the DOS spectra (Refer to **Figure 3.5**). In Figure 6(a and b), we illustrate the electron density distributions of the Highest Occupied Molecular Orbital (HOMO) and the Lowest Unoccupied Molecular Orbital (LUMO) subsequent to the adsorption of Adenine onto the C_{24} fullerene. Notably, these visualizations distinctly reveal the concentration of LUMO electron density residing between the nearest nitrogen atom of Adenine and an adjacent carbon atom of the C_{24} fullerene. This observation serves as compelling evidence for a robust interaction and the formation of a

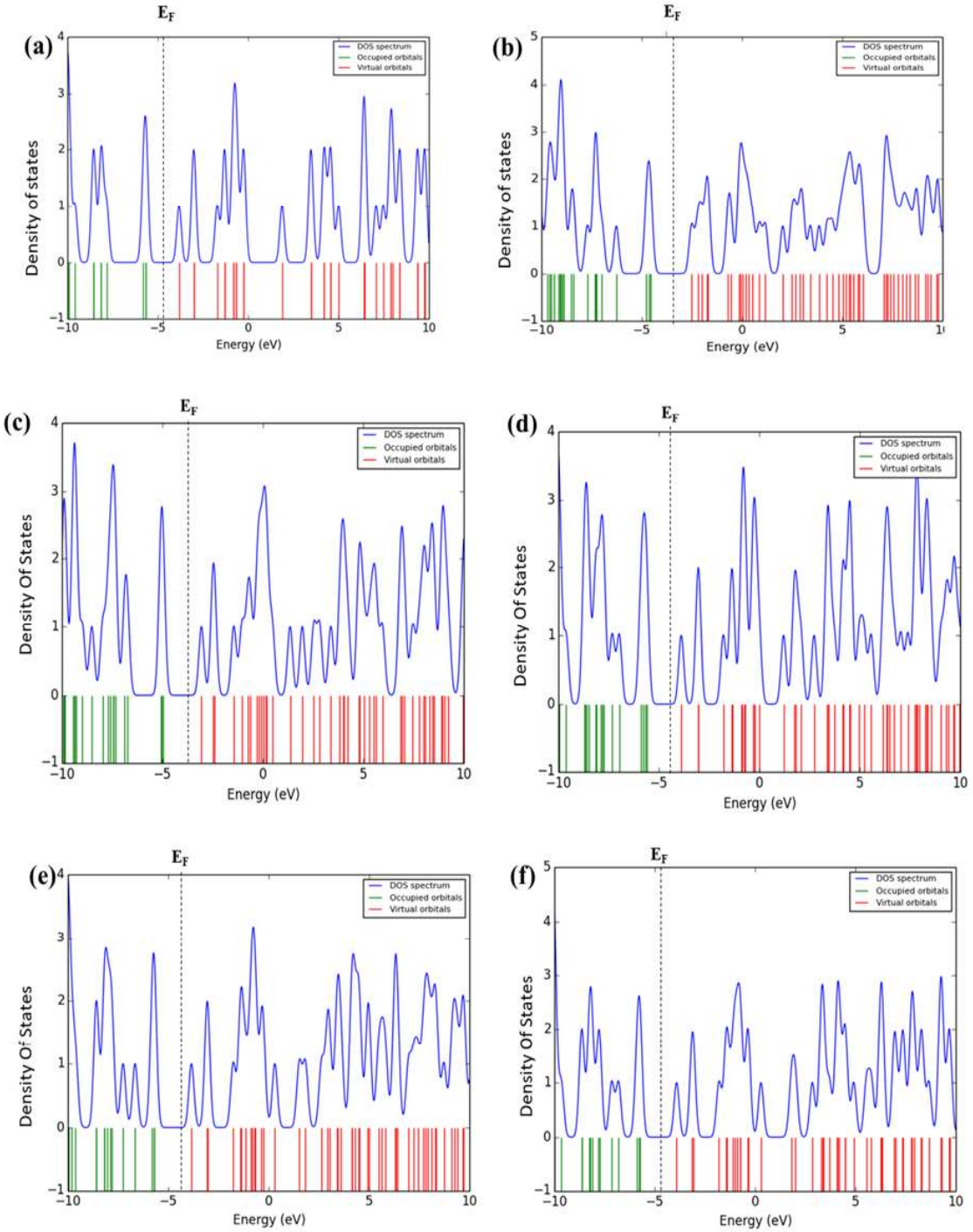

Figure 3.5: *Spectral density of states (DOS) for the C_{24} fullerene (depicted in (a)) and for the nucleobases (Adenine (b), Cytosine (c), Guanine (d), Thymine (e), and Uracil (f)) when adsorbed onto C_{24} fullerenes, respectively.*

chemical bond between Adenine and C_{24} fullerene. Similarly, we observe a comparable localization of HOMO and LUMO electron densities between Cytosine and C_{24} fullerene, aligning seamlessly with the optimal adsorption energy, thus reinforcing the significance of this phenomenon. When it comes to the adsorption of Guanine, Thymine, and Uracil onto C_{24}

fullerene, there is a noticeable absence of substantial electron density distribution between and these molecules and C_{24} fullerene in both the Highest Occupied Molecular Orbital (HOMO) Lowest Unoccupied Molecular Orbital (LUMO) maps. These arrangements closely resemble the pristine C_{24} fullerene (as shown in **Figure 3.6**), underscoring the notion of weak or physisorption characteristics in the adsorption process. Consequently, our qualitative affirmation of nucleobase adsorption onto C_{24} can be supported through Density of States (DOS) analysis, which aligns with the adsorption energy calculations.

3.3.5 Sensing Response

In experimental scenarios, the sensing capabilities are contingent upon the energy gap linked to alterations in the count of conduction electrons, effectively characterizing the adsorbent as a chemical sensor. In our study, we employed a formula for sensing response based on resistivity, which draws inspiration from various references [41-44]. Notably, our analysis revealed that the ultimate sensor sensitivity is exclusively governed by the magnitude of the change in energy gap, denoted as $|\Delta E_G|$. We have provided a comprehensive derivation, and through this method, we calculated the sensing response (S) for the complexes, utilizing an equation that hinges on the band gap, as specified in the referenced derivation [41].

The resistance of the adsorbate (R_1) and the target with the adsorbate (R_2) are found to be connected to the sensing response [43-44];

$$S = |R_2 - R_1|/R_1, \text{----------(4)}$$

where R_2 and R_1 represent the resistivity of C_{24} fullerene and C_{24}/nucleobase complexes, respectively. We may rephrase equation (4) in terms of conductivity since we are aware that resistivity is inversely proportional to conductivity;

$$S = |(\sigma_1/\sigma_2) - 1| \text{----------(5)}$$

The bandgap of an adsorbate directly correlates with both its conductivity and that of the target it is used with [45-47].

$$\sigma = AT^{3/2} \exp(-E_G/KT) \text{--------(6)}$$

Where σ denotes electrical conductivity, A represents a constant, K indicates the Boltzmann constant, and T is the operating temperature. By incorporating equation (6) into equation (5), we arrive at the ultimate expression for the sensing response of the sensor. This expression is

contingent upon the alteration in the band gap that occurs post-interaction, and it is derived as presented in references[41-42].

$$S = \exp(|\Delta E_G| / KT) - 1 \text{----------} (7)$$

Here, ΔE_G represents the difference between E_{G2} and E_{G1}, where E_{G2} corresponds to the energy gap of the C_{24} fullerene, and E_{G1} corresponds to the energy gap of the complex. The electronic configuration of C_{24} fullerene undergoes significant alterations when exposed to Adenine, as depicted in **Table 3.1**. When Guanine is adsorbed, the band gap of C_{24} decreases, resulting in heightened electrical conductivity. Conversely, the adsorption of Adenine and Cytosine leads to an increase in the band gap, resulting in decreased electrical conductivity. However,

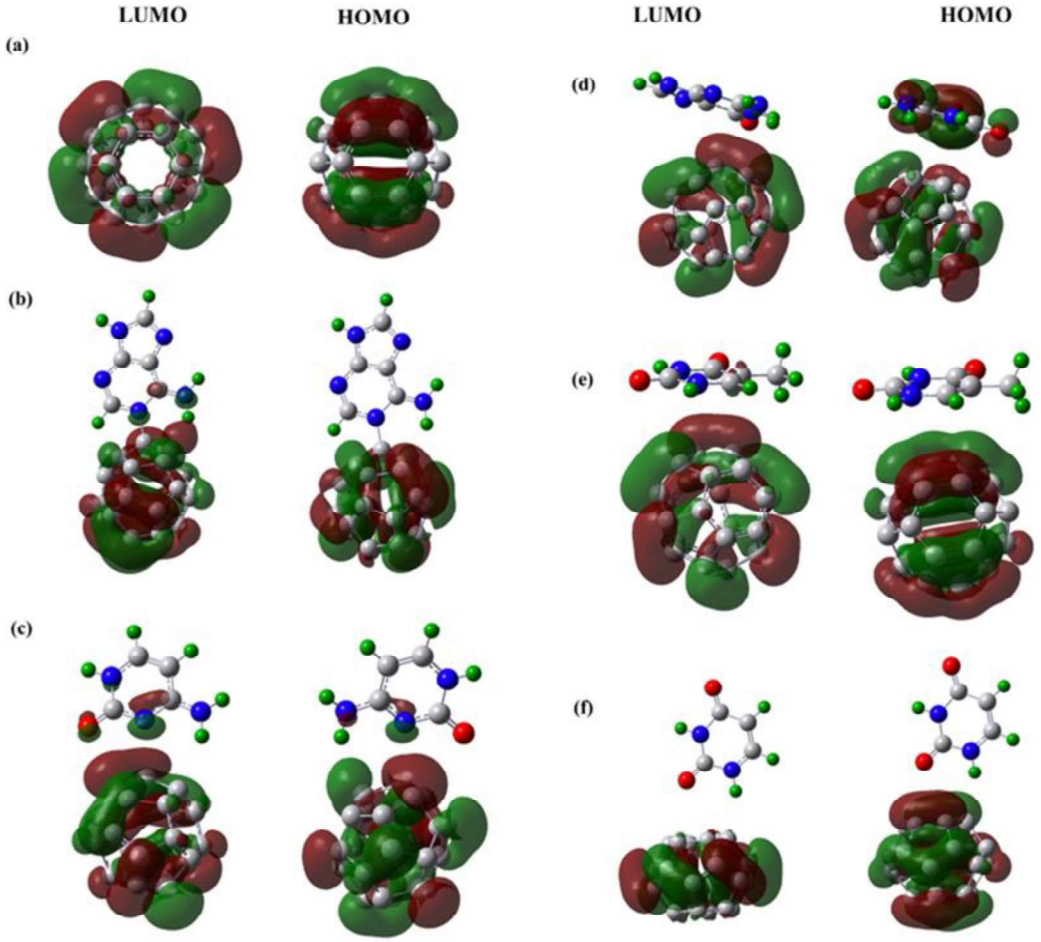

Figure 3.6: *The electron density of the Lowest Unoccupied Molecular Orbital (LUMO) and the Highest Occupied Molecular Orbital (HOMO) for the Pristine C_{24} fullerene (illustrated in (a)), as well as for the nucleobases (Adenine (b), Cytosine (c), Guanine (d), Thymine (e), and Uracil (f)) when adsorbed onto C_{24} fullerene, respectively.*

Thymine and Uracil exhibit minimal reductions in electrical conductivity, indicating a lower affinity for C_{24}. As per equation (7), the sensing response hinges on $|\Delta E_G|$, representing the disparity in band gaps between the pristine C_{24} and C_{24} combined with a nucleobase. Our observations show that Adenine and Guanine display the most substantial difference in band gaps, consequently resulting in the highest sensing response compared to the other nucleobases. This suggests that C_{24} fullerene exhibits effective sensing capabilities when exposed to Adenine and Guanine. Our computed sensing response value for C_{24} fullerene's interaction with Adenine at a temperature of 300 K is approximately 3504.7, signifying that Adenine elicits the most favorable sensing response compared to the other four nucleobase molecules, as detailed in **Table 3.3**. The next most favorable responses are associated with Cytosine and Guanine, while Thymine and Uracil exhibit less promising sensing responses. This is attributed to the absence of significant changes in E_G following their adsorption onto C_{24} fullerene.

Table 3.3: *The computed variations in E_G (ΔE_G), recovery time (τ), and sensing response (S) for Adenine, Cytosine, Guanine, Thymine, and Uracil when they are adsorbed onto C_{24} fullerene, respectively.*

System	ΔE_G (eV)	τ (sec)	S
C_{24}	.....	.....	.....
A/C_{24}	-0.21	3.07×10^{4}	3504.75
C/C_{24}	-0.08	4.41×10^{-14}	21.08
G/C_{24}	+0.10	3.96×10^{-14}	50.71
T/C_{24}	-0.03	3.40×10^{-14}	2.19
U/C_{24}	-0.01	3.16×10^{-14}	0.47

3.3.6 Recovery time

The recovery time plays a vital role in evaluating a biosensor's performance as it provides insights into the desorption process, intimately linked with the strength of interaction. Molecules exhibiting stronger interaction energies with the adsorbent surface tend to have shorter recovery times, whereas those with weaker interactions are less suitable for sensing applications. Hence, achieving an optimal interaction energy level is essential for an effective sensor [31]. The formula for recovery time (τ) is expressed as follows [48]:

$$\tau = \upsilon_0^{-1} \exp(-E_{ad}/KT) \text{----------} (8)$$

In this context, T represents the temperature (300K), K signifies Boltzmann's constant, and υ_0 corresponds to the attempt frequency. Experimental studies on the desorption of biomolecules

and drugs have demonstrated the use of various photonic frequencies (υ_0) or thermal energies [49]. We can forecast the recovery times for Adenine, Cytosine, Guanine, Thymine, and Uracil as they disengage from the surface of C_{24} fullerene by choosing a photonic frequency of 10^{15} s^{-1} and a temperature of 300K (see **Table 3.3**). Adenine had a maximum recovery time of 3.07 $\times 10^4$ s, which was predicted given their significant chemisorption. This prolonged Recovery time indicates that the C_{24} fullerene can be used to remove adenine from the series of nucleobases. The CRISPR/Cas9 technique, which has been extensively employed recently for gene editing and sequencing, uses this kind of process [50]. A shorter interatomic distance of 2.38 and 2.79 from the C_{24} fullerene, as well as lower recovery durations of 4.41×10^{-14} s and 3.96×10^{-14} s, for cytosine and guanine, respectively, imply that these two molecules might be employed for the best detection for the C_{24} biosensor.

3.3.7 Solvent Effect

To account for the relevance of the biological environment, we conducted investigations into the influence of solvents on the adsorbate-adsorbent complexes. We employed the polarizable continuum model (PCM) method, a method with significant implications in understanding the behaviors of these complexes in actual biological settings [51]. Our approach involved separate re-optimization of all five nucleobase molecules, C_{24} fullerene, and the minimum configurations of A, C, G, T, U, and C_{24} complexes in a water environment. This was achieved using the DFT/B3LYP/6-31(d,p) method with Grimme's dispersion corrections (D3 version). **Table 3.4** lists the computed values for adsorption energies, sensing reactions (S), and recovery times (τ).

The results suggest that with an increase in solvent electric permittivity, the overall energy levels of the C_{24} fullerene, Adenine, and Cytosine system trend lower. This leads to an enhanced adsorption energy for the A/C_{24} and C/C_{24} complexes compared to their behavior in a gaseous phase, resulting in respective adsorption energies of -1.35 eV and -1.36 eV [38]. On the contrary, the adsorption energy of G/C_{24}, T/C_{24}, and U/C_{24} complexes diminishes under the influence of the solvent, signifying their decreased stability in a water-based milieu. In the case of A/C_{24} and C/C_{24} complexes, the increased interaction energy observed in a water environment signifies enhanced stability. This heightened stability is also reflected in higher sensing responses and longer recovery times, as outlined in **Table 3.4**. Furthermore, to assess

the solubility of Adenine and Cytosine in water, we computed the solvation energies (ΔE_{sol}) using the following equation [41]:

$$\Delta E_{sol} = E_{sol} - E_{gas} \text{----------(9)}$$

Table 3.4: *Calculated value of Adsorption energy (E_{ad}), LUMO energy (E_{LUMO}), HOMO energy (E_{HOMO}), HOMO-LUMO gap (E_G), Recovery Time (τ) and Sensing Response (S) for Adenine, Cytosine, Guanine, Thymine and Uracil adsorbed C_{24} fullerene with solvent effect, respectively.*

System	E_{ad} (eV)	E_{LUMO} (eV)	E_{HOMO} (eV)	E_G (eV)	τ (sec)	S
C_{24}	…..	-3.76	-5.59	1.83	….	…..
A/C_{24}	-1.35	-2.67	-4.72	2.05	5.37×10^{7}	4964.69
C/C_{24}	-1.36	-2.52	-4.58	2.07	6.04×10^{7}	10763.12
G/C_{24}	-0.32	-3.73	-5.49	1.76	2.67×10^{-10}	13.99
T/C_{24}	-0.30	-3.73	-5.57	1.84	1.55×10^{-10}	0.472
U/C_{24}	-0.22	-3.77	5.61	1.84	1.55×10^{-10}	0.472

This equation evaluates ΔE_{sol}, where E_{sol} represents the system's energy in a water solvent, and E_{gas} represents the energy in a gas phase. The computed ΔE_{sol} values for Adenine and Cytosine are -0.37 eV and -0.57 eV, respectively. For C_{24} fullerene, ΔE_{sol} is -0.021 eV. The lower solubility of C_{24} fullerene in water is evident from its lower solvation energy. In contrast, the solvation energies (ΔE_{sol}) for Adenine/C_{24} and Cytosine/C_{24} complexes are -0.19 eV and -0.94 eV, respectively, suggesting their higher solubility in a water environment. These findings reveal that the solvation energy of the Adenine/C_{24} complex is lower than the sum of the solvation energies of Adenine and C_{24} fullerene individually. This suggests that both Adenine and C_{24} fullerene are more soluble in strongly polar environments and exhibit lower solubility in water, especially when compared to Cytosine. Additionally, it's noteworthy that the energy gap of nucleobases adsorbed onto C_{24} fullerene experiences a slight increase in a watery environment compared to the gas phase. When exposed to adenine and cytosine, C_{24}'s sensing response increases from 3504.75 and 21.08 in gas to 4964.69 and 107663.12 in water. However, Guanine, Thymine, and Uracil were discovered to have interaction energies that were reduced

as a result of the solvent effect, indicating that these nucleobase complexes are less reactive and less stable in water. They are used for detection because of their quicker recovery time.

3.3.8 Dipole Moment

The Dipole moment (μ) holds significance in assessing how adsorbates and substrates interact with their surroundings [51]. **Table 3.5** displays the dipole moments for C_{24} fullerene and its complexes with the five nucleobases in both gaseous and aqueous phases. In the gas phase, C_{24} exhibits a dipole moment of 0.0035 D (Debye). The dipole moment is shown to significantly change after the absorption of adenine, cytosine, guanine, thymine, and uracil onto C_{24}, with values of 12.23 D, 9.26 D, 5.52 D, 3.74 D, and 3.68 D, respectively. A > C > G > T > U is the order in which the adsorption energy (E_{ad}) is greatest for the nucleobases on C_{24}. This sequence is in line with the general pattern. This increased dipole moment attests to the strong interaction between these elements. As seen in Table 5, a similar trend may be seen for the aqueous phase. After the nucleobases are adsorbed, the dipole moment of C_{24} increases. The order of the dipole moment and the interaction energy follows the same trend. Following adenine, Cytosine and Guanine are found to have the best interaction energy and the shortest interatomic distance over C_{24} fullerene. These findings validate C_{24}'s effective detection of adenine, cytosine, and guanine in the gaseous phase. In contrast to cytosine and guanine, however, adenine takes longer to separate from C_{24}. These nucleobases can be distinguished from one another due to the variation in adsorption energy and recovery time. The C_{24} may be utilized for both removal and carrier application, according to the increase in adsorption energy and recovery time of adenine and cytosine in water.

Table 3.5: *Dipole moments of Adenine, Cytosine, Guanine, Thymine, and Uracil when adsorbed onto C_{24} fullerene, both in the absence (μ_{gas}) and presence (μ_{water}) of solvent effect*

System	μ_{gas} (Debye)	μ_{water} (Debye)
C_{24}	0.0035	0.00022
A/C_{24}	12.23	20.39
C/C_{24}	9.26	24.94
G/C_{24}	5.52	8.51
T/C_{24}	3.74	5.62

3.4 Conclusion

In the current work, the gas phase adsorption behavior and mechanism of nucleobases on C_{24} fullerene as well as the influence of the solvent were studied. Our findings show that the Adenine and C_{24} fullerene exhibit a robust chemical interaction in the gas phase, which suggests a stronger sensing response and a longer recovery period. This shows that the C_{24} fullerene may be used as a DNA biosensor to separate adenine from the other DNA nucleobase units. Cytosine, Guanine, Thymine, and Uracil are seen to be adsorbed on the C_{24} fullerene through a process known as physisorption, which results in recovery durations of just 10^{-14} s and minimal sensing responses. Cytosine and Guanine among all investigated nucleobase have optimal interaction energies and shorter interatomic distances over C_{24} fullerene, proposing as a useful detector for them. A weak interaction between thymine and uracil with C_{24} in the order T > U is confirmed by the electrical and adsorption analyses. Additionally, the adsorption energy of the cytosine and adenine complexes rises with the solvent effect in comparison to the gaseous phase, confirming that the complexes are more reactive and stable in the water medium. Adenine/C_{24} is less soluble in water because its solvation energy is lower than that of pure C_{24}. The sensing responses and recovery times for adenine and cytosine are noticeably accelerated. These nucleobases (Adenine and Cytosine) might be removed from water using the C_{24} biosensor. In the instance of interactions involving guanine, thymine, and uracil, it has been discovered that the interaction energy has reduced owing to the solvent effect. This means that these nucleobase complexes are less reactive, leading to shorter recovery times, and may thus be employed for detecting purposes. The C_{24} fullerene is a viable option for nucleobase sensing applications, and it may be utilized to accurately predict the nucleobase sequence in a DNA/RNA strand, we conclude.

References:

1 A. Sassolas, B. D. Leca-Bouvier and L. J. Blum, *Chem. Rev.*, 2008, **108**, 109–139.

2 W. Suginta, P. Khunkaewla and A. Schulte, *Chem. Rev.*, 2013, **113**, 5458–5479.

3 K.K. Hamed, R. Vahideh, E. Ali and S. Fatemeh, *J. Cell Dev. Biol.*, 2020, **3**, 28–35.

4 P. Mehrotra, *J. Oral Biol. Craniofacial Res.*, 2016, **6**, 153–159.

5 E. C. Anota, Y. Tlapale, M. S. Villanueva and J. A. R. Márquez, *J. Mol. Model.*, 10.1007/s00894-015-2768-0.

6 A. D. O. Muñoz, A. Escobedo-Morales, E. Skakerzadeh and E. C. Anota, *J. Mol. Liq.*, 2021, **322**, 114951.

7 X. J. Wang and Z. Liu, *Chinese Sci. Bull.*, 2012, **57**, 167–180.

8 Y. V. Shtogun, L. M. Woods and G. I. Dovbeshko, *J. Phys. Chem. C*, 2007, **111**, 18174–18181.

9 M. T. Baei, M. R. Taghartapeh, E. T. Lemeski and A. Soltani, *Phys. B Condens. Matter*, 2014, **444**, 6–13.

10 A. Hirsch, *Angew. Chemie Int. Ed. English*, 1993, **32**, 1138–1141.

11 R. B. Ross, C. M. Cardona, D. M. Guldi, S. G. Sankaranarayanan, M. O. Reese, N. Kopidakis, J. Peet, B. Walker, G. C. Bazan, E. Van Keuren, B. C. Holloway and M. Drees, *Nat. Mater.*, 2009, **8**, 208–212.

12 J. Ma, Q. Guo, H. L. Gao and X. Qin, *Fullerenes Nanotub. Carbon Nanostructures*, 2015, **23**, 477–482.

13 H. Kroto, *Science (80).*, 1988, **242**, 1139–1145.

14 S. T. Zuckerman and W. J. Kao, *Nanomaterials and Biocompatibility: Carbon Nanotubes and Fullerenes*, 2009.

15 S. V. Lokesh, B. S. Sherigara, Jayadev, H. M. Mahesh and R. J. Mascarenhas, *Int. J. Electrochem. Sci.*, 2008, **3**, 578–587.

16 F. Xiao, Z. Chen, Z. Wei and L. Tian, *Adv. Sci.*, 2020, **7**, 1–34.

17 A. Shokuhi Rad, Y. M. Jouibary, V. P. Foukolaei and E. Binaeian, *Curr. Appl. Phys.*, 2016, **16**, 527–533.

18 A. Shokuhi Rad and K. Ayub, *J. Alloys Compd.*, 2016, **672**, 161–169.

19 J. Shi, Y. Liu, L. Wang, J. Gao, J. Zhang, X. Yu, R. Ma, R. Liu and Z. Zhang, *Acta Biomater.*, 2014, **10**, 1280–1291.

20 N. P. Shetti, S. J. Malode and S. T. Nandibewoor, *Bioelectrochemistry*, 2012, **88**, 76–83.

21 D. Y. Lyon, L. K. Adams, J. C. Falkner and P. J. J. Alvarez, *Environ. Sci. Technol.*, 2006, **40**, 4360–4366.

22 A. Shokuhi Rad and K. Ayub, *Comput. Theor. Chem.*, 2017, **1121**, 68–75.

23 C. A. Celaya, L. F. Hernández-Ayala, F. Buendía Zamudio, J. A. Vargas and M. Reina, *J. Mol. Liq.*, 10.1016/j.molliq.2021.115528.

24 B. T. Tomić, C. S. Abraham, S. Pelemiš, S. J. Armaković and S. Armaković, *Phys. Chem. Chem. Phys.*, 2019, **21**, 23329–23337.

25 F. Yaghoobi, S. Salehzadeh and M. Maddah, *J. Mol. Liq.*, 2020, **301**, 112339.

26 S. Grimme, J. Antony, S. Ehrlich and H. Krieg, *J. Chem. Phys.*, 10.1063/1.3382344.

27 M.J. Frisch, G.W. Trucks, H.B. Schlegel, G.E. Scuseria, M.A. Robb and et al G. Scalmani, V. Barone, B. Mennucci, G.A. Petersson, *Gaussian 09, Revis. D.01, Gaussian Inc., Wallingford, CT,*.

28 J. J. Adjizian, A. Vlandas, J. Rio, J. C. Charlier and C. P. Ewels, *Philos. Trans. R. Soc. A Math. Phys. Eng. Sci.*, 10.1098/rsta.2015.0323.

29 M. Rakib Hossain, M. Mehade Hasan, S. Ud Daula Shamim, T. Ferdous, M. Abul Hossain and F. Ahmed, *Comput. Theor. Chem.*, 2021, **1197**, 113156.

30 C. Parlak and Ö. Alver, *Chem. Phys. Lett.*, 2017, **678**, 85–90.

31 M. A. Hossain, M. R. Hossain, M. K. Hossain, J. I. Khandaker, F. Ahmed, T. Ferdous and M. A. Hossain, *Chem. Phys. Lett.*, 2020, **754**, 137701.

32 S. Vadalkar, D. Chodvadiya, N. N. Som, K. N. Vyas, P. K. Jha and B. Chakraborty, *ChemistrySelect*,10.1002/slct.202103874.

33 M. Shahabi and H. Raissi, *J. Incl. Phenom. Macrocycl. Chem.*, 2015, **84**, 99–114.

34 M. Shahabi and H. Raissi, *J. Incl. Phenom. Macrocycl. Chem.*, 2016, **86**, 305–322.

35 C. Parlak and Ö. Alver, *J. Mol. Struct.*,10.1016/j.molstruc.2019.126881.

36 S. Demir and M. F. Fellah, *Appl. Surf. Sci.*,10.1016/j.apsusc.2019.144141.

37 R. Chandiramouli, A. Srivastava and V. Nagarajan, *Appl. Surf. Sci.*, 2015, **351**, 662–672.

38 M. Yoosefian and N. Etminan, *Amino Acids*, 2018, **50**, 653–661.

39 F. Kamali, G. Ebrahimzadeh Rajaei, S. Mohajeri, A. Shamel and M. Khodadadi-Moghaddam, *Monatshefte fur Chemie*, 2020, **151**, 711–720.

40 A. S. Rad and S. M. Aghaei, *Curr. Appl. Phys.*, 2018, **18**, 133–140.

41 J. Jiang, T. Yan, D. Cui, J. Wang, J. Shen, F. Guo and Y. Lin, *J. Mol. Liq.*, 2020, **315**, 113741.

42 Y. Yang, A. Sun and M. Eslami, *Phys. E Low-Dimensional Syst. Nanostructures*, 2021, **125**, 114411.

43 P. Dipak, D. C. Tiwari, A. Samadhiya, N. Kumar, T. Biswajit, P. A. Singh and R. K. Tiwari, *J. Mater. Sci. Mater. Electron.*, 2020, **31**, 22512–22521.

44 D. C. Tiwari, P. Atri and R. Sharma, *Synth. Met.*, 2015, **203**, 228–234.

45 M. Eslami and A. A. Peyghan, *Thin Solid Films*, 2015, **589**, 52–56.

46 A. A. Peyghan and M. Noei, *Phys. B Condens. Matter*, 2014, **432**, 105–110.

47 M. T. Baei, A. A. Peyghan and Z. Bagheri, *Struct. Chem.*, 2013, **24**, 1099–1103.

48 J. Li, Y. Lu, Q. Ye, M. Cinke, J. Han and M. Meyyappan, *Nano Lett.*, 2003, **3**, 929–933.

49 R. Kumar, N. Goel and M. Kumar, *ACS Sensors*, 2017, **2**, 1744–1752.

50 J. A. Doudna and E. Charpentier, *Science (80).*, 10.1126/science.1258096.

51 M. Cossi, V. Barone, R. Cammi and J. Tomasi, *Chem. Phys. Lett.*, 1996, **255**, 327–335.